

Assessment of the Limits of Tabular Aerodynamic Models for Flight Dynamics Analysis using the SACCON UCAV Configuration

D. Vallespin, * M. Ghoreyshi [†] & K.J. Badcock [‡]

Department of Engineering, University of Liverpool, Liverpool, UK L69 3BX, United Kingdom

This paper describes the assessment of tabular aerodynamic models for flight dynamics purposes done using CFD methods. A generic UCAV model is used. Experimental data was used to validate the predictions. The flow topologies and resulting forces and moments were investigated with good agreement between the sources. The tabular models were then generated. To reduce computational cost, kriging and data fusion were used to populate the tables using only a relatively small number of CFD calculations. Once the tables were complete, these were used to calculate a set of manoeuvres. The result was a set of time optimum manoeuvres which were then replayed through the time accurate CFD code. The assessment of the tabular method was then carried out by comparing the force and moment data obtained from the CFD replay with those in the tables.

I. Introduction

From the flight dynamics perspective the use of CFD has great potential to predict manoeuvring capabilities of aircraft. Simulation can be used at different levels of computer cost, from generating the linear equations of motion through to populating tabular models or simulating manoeuvres using time accurate CFD calculations.

The flight mechanics analysis of UCAV configurations requires an accurate prediction of the flow behaviour around it. The performance of a conventional UCAV configuration displays nonlinear aerodynamic effects, arising from vortical flow. These are described in a recent review¹ where vortical flows are seen to adopt different behaviour according to the wing sweep angle. CFD can be used to construct and assess tabular aerodynamic models.

The validity of the tables can be limited by strong history effects. To test this, time accurate CFD calculations are available to replay manoeuvres for comparison with the tabular forces and moments. Such a study was carried out by Ghoreyshi² for the Standard Dynamics Model (SDM) where a range of manoeuvres were computed using the Euler equations and the forces and moments compared with those from a tabular model.

The current study looks to extend this earlier work by considering table generation and motion replay based on the Reynolds Averaged Navier-Stokes (RANS) equations. This is done for a test case, the SACCON UCAV, that has experimental data available. The paper continues with a description of the test case and the CFD code. Then the table and manoeuvre generation is considered, following which the replay of several manoeuvres is shown. Finally conclusions are given.

II. Model Description

The SACCON UCAV geometry consists of a lambda wing with a reference chord of $0.479m$, a sweep angle of 53° and a wing washout of 5° . Two leading edge geometries were designed for this model, one that was round (RLE) and a sharp one (SLE). The RLE has a blend from a sharp to a round shape from the apex

*PhD Student, Dept. of Engineering, University of Liverpool

[†]Research Associate

[‡]Professor, Dept. of Engineering, University of Liverpool

to the tip, respectively, whereas the SLE consisted of a wedge which decreased in thickness towards the tip of the wing. Both the tip and the trailing edge are blunt. For the purpose of this paper only the SLE model is used. Wind tunnel experiments were carried out on the SACCON at the DNW Braunschweig facilities.³ This is a low speed, closed section wind tunnel with dimensions of $3.25m \times 2.8m$. The testing campaign consisted of a series of static and dynamic runs. The static tests were carried out for a range of angles of attack at different sideslip angles. The dynamic cases were pitching, yawing and plunging motions at frequencies of 1, 2 and 3Hz and amplitudes of 5° . The rotations in the dynamic runs were done about a point on the x-axis, $x = 0.85m$. Pressure measurements on the surface of the model were taken using pressure taps and kulites. Particle Image Velocimetry (PIV) was used to take flow field velocity measurements at different cross sections along the chord of the model. Finally, the sensors in the belly sting mounting measured the total forces and moments on the body. The Moment Reference Point (MRP) was chosen to be at $0.6m$ along the axis of symmetry. The data from the experiments was used to validate the predictions from the structured CFD solver used, described in section III. In order to make these predictions, a full span, 10 million point, structured multiblock grid was generated using ICEM CFD.⁴ A H-type blocking is used around this configuration to provide the best cell quality around the leading edge geometry of the SLE model, Fig 1 (a). The sting mounting was not included in the CFD model for simplicity.

In order to compute the manoeuvres a pair of control surfaces were included in the geometry. These covered most of the wing section's span along the trailing edge and 20% of the chord, as shown in Figure 1 (a). The way in which they were modelled in the CFD was by allowing the surface mesh to deform to the desired position and accommodating the grid points in the surrounding blocks to the new geometry. Figure 1 (b) shows a screenshot of the SACCON's deformed control surface mesh. The red and blue grids represent the maximum and minimum deflections, respectively.

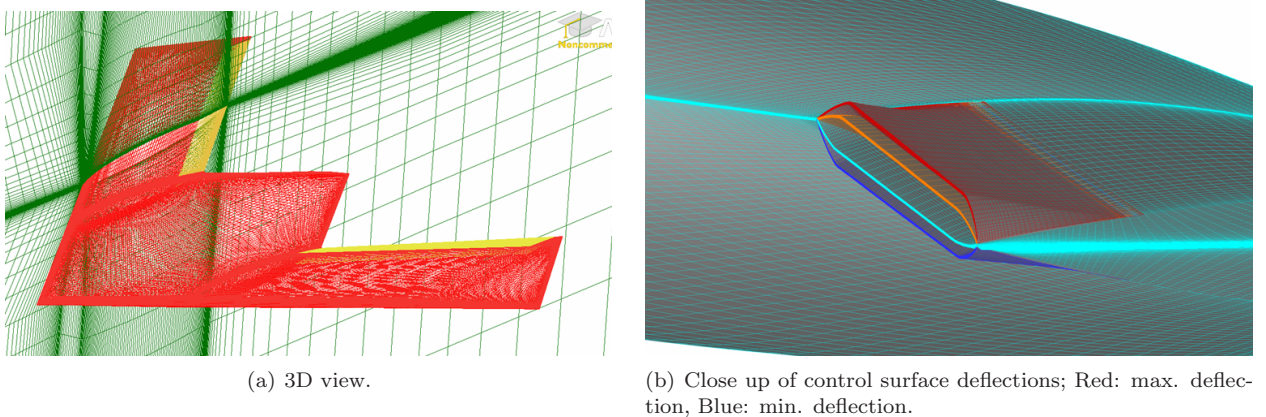


Figure 1. SACCON SLE grid with control surface implemented.

III. Flow Solver

The parallel multiblock (PMB) solver⁵ was the solver used for the purpose of this study. Unsteady dynamic calculations are possible which were used to perform dynamic oscillations about the chosen centre of gravity and calculate the dynamic derivatives of the model. Manoeuvres can be replayed in this time accurate manner by specifying the UCAV flight trajectories through any given manoeuvre. The Euler and Reynolds-averaged Navier-Stokes (RANS) equations are discretised on curvilinear, multiblock, body-conforming grids using a cell-centred finite volume method that converts the partial differential equations into a set of ordinary differential equations. The convective terms are discretised using Osher's upwind method. A monotone upwind scheme for conservation laws variable extrapolation is used to provide second-order accuracy with the Van Albada limiter to prevent spurious oscillations around shock waves. Following Jameson, the spatial residual is modified by adding a second-order discretisation of the real time derivative to obtain a modified steady-state problem for the flow solution at the next real time step. The linear system is solved in an unfactored form using a Krylov subspace method with block incomplete upper lower preconditioning. The preconditioner is decoupled between blocks to allow a high efficiency on parallel

computers with little detriment to the convergence of the linear solver. For the Jacobian matrix of the CFD residual function, approximations are made that reduce the size and improve the conditioning of the linear system without compromising the stability of the time marching. While the dynamic derivatives were calculated based on Euler dynamic calculations, the tables and manoeuvre replays were computed using RANS. The turbulence model used to generate these predictions was the baseline $k-\omega$ model.⁶ This model utilises the Wilcox model in the inner 50% of the boundary layer and gradually changes to $k-\epsilon$ towards the boundary layer edge.⁷

IV. CFD Validation

Comparisons of integral force and moment data as well as pressure coefficient distributions and PIV measurements were made for the SACCON SLE and RLE models.⁸ The flow around the SACCON is highly nonlinear due to the vortical structures occurring over the top surface at high angles of attack. For the purpose of this study, only the SLE model will be discussed. Based on the CFD results, the SLE configuration had a two-vortex structure occurring, one at the apex of the wing which travelled in the downstream and spanwise directions and the second at the tip section. The outboard vortex started to occur at an incidence of 10° whereas the presence of the apex vortex became evident at 12.5° , Fig 2. As the angle of attack was increased both of these were seen to become stronger and the outboard vortex to travel inwards. At 14° the two vortices were so close they were barely distinct from each other and by 15° of incidence there was no trace of the dual vortex structure. Beyond this point the flow topology of the SACCON SLE resembled that of a typical high sweep delta wing. Overall the forces and moments originating from this show a linear

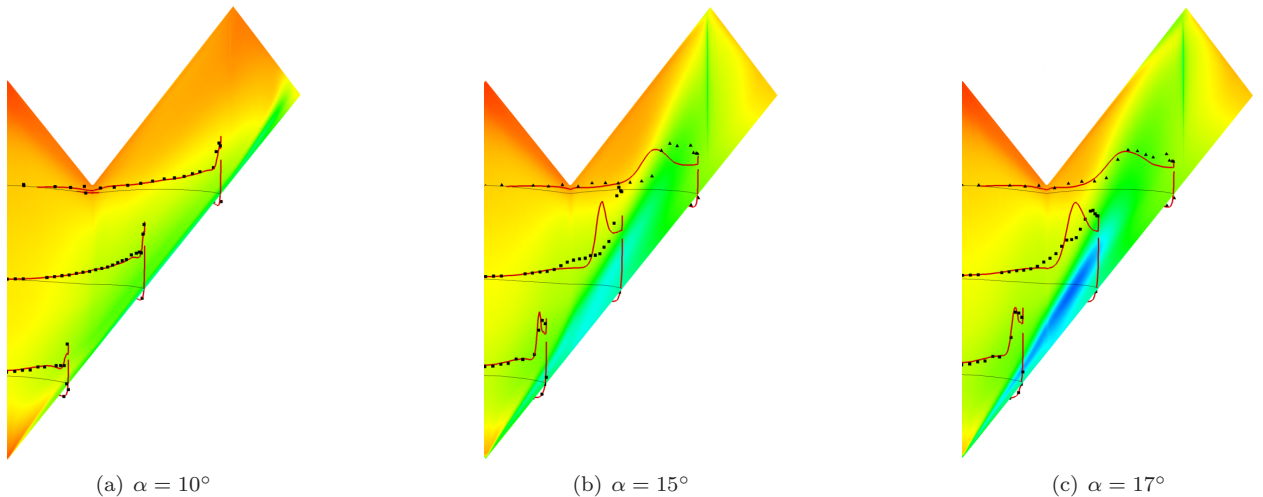
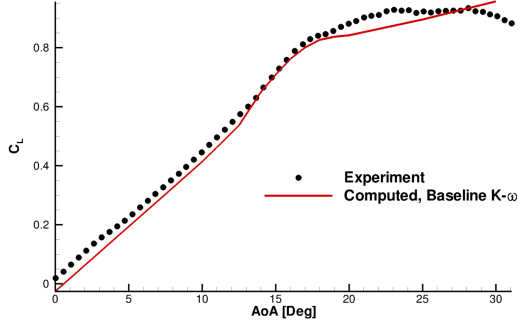


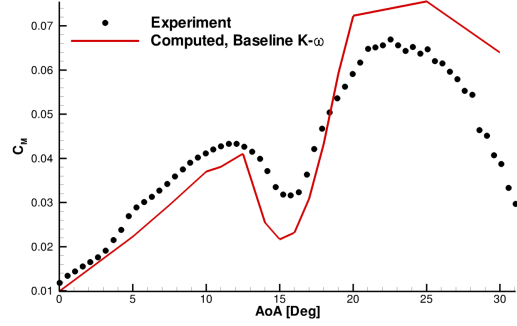
Figure 2. Predicted pressure coefficient distribution with 3D crossplots of experimental and other CFD data for the SLE.

trend up to angles of attack around 10° , after which the moment coefficient curve dips considerably before increasing again, Fig 3 (b). This dip in the moment curve is due to the sudden jump in the tip vortex position as it travels inboard with increasing angle of attack. The lift coefficient curve shows a linear trend up to an angle of 12.5° before the first signs of wing stall occur. The agreement with the measured force and moment coefficients is good in the linear region, as shown by the black symbols in Fig 3. The coefficients show an offset with the experiments which is likely to be due to the belly sting mounting.⁹ The dip in the moment curve is weaker in the experimental measurements whereas for the higher angles, the CFD tends to overpredict the value of the pitching moment. A slight increase in disagreement in the lift coefficient can be seen around 22° angle of attack. The predicted vortex positions throughout the alpha sweep is the main reason for this disagreement. As a general rule, the measurements show the vortices staying closer to the leading edge, Fig 2. The CFD on the other hand struggles to predict a realistic flow separation line, particularly around the blunter part of the leading edge where this is not fixed at the leading edge.⁸

Overall, the forces and moments predicted by the $k\omega$ model are in reasonable agreement with the measurements. Most importantly, the main flow characteristics are well captured in the predicted integral data



(a) Lift coefficient against angle of attack.



(b) Pitching moment coefficient against angle of attack.

Figure 3. Integral data from experimental results and PMB computations for the SACCON model.

plots. This is satisfactory for the purpose of the flight dynamics study. The CFD results show important hysteresis effects in the dynamic results, in particular at mean angles of attack of 15° and 20° . These flow transients occurring as the UCAV attitude changes are one of the key phenomena in the comparison of tabular methods and time accurate CFD calculations.

V. Table Generation and Flight Dynamic Model

The generation of the aerodynamic data tables was carried out based on sampling and data fusion.¹⁰ This approach uses a small number of high quality predictions to reproduce the behaviour throughout the flight envelope. The first set of samples is taken at the extremes of the flight envelope to avoid the need for extrapolation whilst populating the tables. Other table locations are then generated by fitting a kriging function between samples. This approach calculates the mean square error (MSE) to determine the distance in the parameter space from the nearest sample. An expected improvement function (EIF) gives an estimation of where the function prediction may be improved. This is used to locate the regions of nonlinearity in the forces and moments. A combination of these two measures places the next sample for calculation. The process finishes when the value of the MSE reaches the specified tolerance or the number of desired steady state calculations is exceeded.

The tables generated for the SACCON model consist of two matrices of three variables:

- [Mach, α and β]
- [Mach, α and $\delta_{aileron}$]

The first is dependent on the Mach number, the angle of incidence and the sideslip angle whereas the second one depends on the Mach number, the incidence and the aileron deflection angle. The flight envelope of the aircraft is defined by the ranges used for the variables in the tables, which were:

- $0.1 < M < 0.3$
- $-15^\circ < \alpha < 30^\circ$
- $-15^\circ < \beta < 15^\circ$
- $-15^\circ < \delta_{aileron} < 15^\circ$

Each table has over 4200 entries, each one consisting of forces and moments in wind axes. 60 steady state calculations were used for the sideslip table at the boundaries and in the regions of nonlinearity. Using co-kriging, the table with aileron deflection was generated using fewer samples. This method takes the behaviour from the sideslip table and uses it as a baseline. The new samples based on the control deflections are generated and used together with trend information from the baseline table.

The flight dynamics model was built using the tables of aerodynamic forces and moments previously described, along with estimations of the geometric parameters, centre of gravity, mass, moments of inertia and dynamic derivatives. The SACCON wind tunnel model was scaled up to fit the characteristics of a full scale aircraft. Estimations of the mass and moments of inertia were made, following work carried out in the Garteur AG47 group based on the Northrop YB-46 aircraft.

mass	2000kg
MAC	5.011m
Root Chord	8.97m
cg	0.4MAC
Span	13m
Ref. Area	55.08m ²
I_{xx}	8014.859kgm ²
I_{yy}	6564.918kgm ²
I_{zz}	8937.279kgm ²

Initially, the centre of gravity (cg) was located at the moment reference point (MRP) for the experiments, 0.6m along the root chord from the apex. This results in a longitudinally unstable aircraft and, for this reason, this point was moved forward, to 0.4m. The single pair of control surfaces modelled in the tables is used as an aileron to control rolling moments. In order to control the pitching and yawing moments thrust vectoring is used. Even though the engine is not modelled in the CFD in this particular study, the optimisation software assumes there is a source of thrust acting at the back of the axis of symmetry. This thrust vector can rotate by up to 45° in the vertical and horizontal axes, thus allowing for pitch and yaw control.

We use the optimal control approach,^{11,12} that finds the optimal controls that transfer a system from the initial state to the final state while minimizing (or maximizing) a specified cost function.¹³ The optimal control aims to find a state-control pair $x^*(t), u^*(t)$ and possibly the final event time t_f that minimizes the cost function

$$J[x(t), u(t), t_0, t_f] = E(x(t_0), u(t_f), t_0, t_f) + \int_{t_0}^{t_f} F(x(t), u(t), t) dt \quad (1)$$

where $x \in R^n$ and $u \in R^m$. The function E and F are endpoint cost and Lagrangian (running cost), respectively. The minimization is subject to the dynamic constraint,

$$\dot{x}(t) = f(x(t), u(t)), \quad t \in [t_0, t_f] \quad (2)$$

and boundary conditions

$$\psi_0[x(t_0), t_0] = 0 \quad (3)$$

$$\psi_f[x(t_f), t_f] = 0 \quad (4)$$

where $\psi_0 \in R^p$ and $\psi_f \in R^q$ with $p, q \leq n$.

The possible state-control path constraints are formulated as

$$h(x(t), u(t), t) \leq 0, \quad h \in R^r \quad (5)$$

where $\partial h / \partial u$ and $\partial h / \partial x$ have full rank.¹⁴

Implementation of the Lagrange multiplier theory for this problem helps to combine the state equation and constraints to the cost function using the time-dependent multipliers $\lambda(t)$ and constant multipliers $\nu_0 \in R^p$ and $\nu_f \in R^q$ to form the augmented cost function:

$$\int_{t_0}^{t_f} [F(x, u) + \lambda^T f[x(t), u(t)] - \dot{x} + \mu^T h(t)] dt \quad (6)$$

where, variable $\lambda(t)$ is named costate variable and represents the increment to F resulting from a marginal increase in state parameters. In terms of the augmented Hamiltonian defined as:

$$H = F(x(t), u(t), t) + \lambda^T f(x(t), u(t), t) + \mu^T h(t) \quad (7)$$

the necessary conditions for optimality are:

$$\frac{\partial H}{\partial u} = 0, \quad \mu^T h = 0, \quad \mu \geq 0 \quad (8)$$

where λ^T needs to satisfy the following equations:

$$\dot{\lambda} = -\frac{\partial H}{\partial x} \quad (9)$$

$$\lambda(t_0) = -\left[\frac{\partial \psi_0}{\partial x(t_0)}\right]^T \nu_0 \quad (10)$$

$$\lambda(t_f) = \frac{\partial E}{\partial x(t_f)} + \left[\frac{\partial \psi_f}{\partial x(t_f)}\right]^T \nu_f \quad (11)$$

$$(12)$$

There are many different methods for solving optimal control problems. In the current paper, the DIDO code¹⁵ and MATLAB¹⁶ are used. In DIDO, the total time history is divided into N segments, spaced using shifted Legendre-Gauss-Lobatto (LGL) rule.¹⁷⁻¹⁹ The boundaries of each time segment are called nodes.

For the problem of an aircraft optimal time manoeuvre, the general aircraft equations of motion detailed in Etkin²⁰ and Stevens and Lewis²¹ serve as one of the constraints. Hence, the state space has twelve state parameters, which, the initial and final state parameters are fixed with trimmed flight conditions, but the rest of the manoeuvre is out of trim conditions.

VI. Manoeuvre Analysis

A. Lazy eight

A half lazy eight manoeuvre generated using DIDO and the full six degree of freedom tabular model is presented. Once the manoeuvres are generated, the time history of states is used to force a replay through the time accurate PMB code. The flight path followed by the aircraft to perform the manoeuvre is shown in Fig. 4. The objective is to turn the aircraft 180° by pulling up, turning and diving to the original altitude.

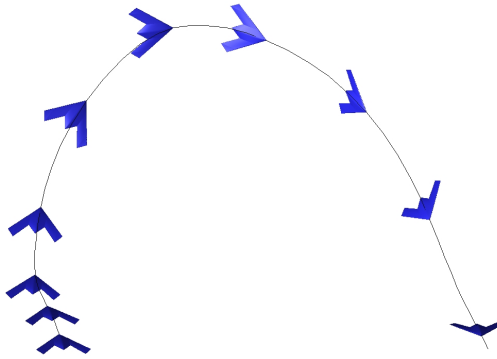
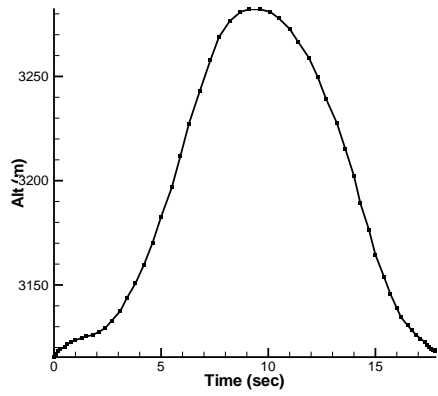
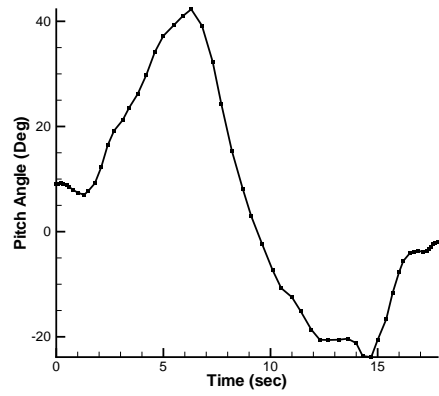


Figure 4. Lazy eight flight path.

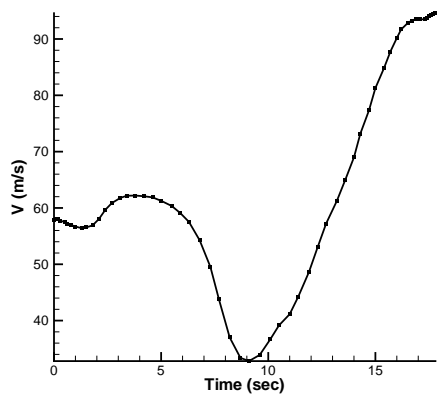
Figure 5 represents the manoeuvre in terms of the angles of roll and pitch, velocity and altitude. From Fig. 5(a) the aircraft can be seen to increase in altitude and return to the initial value at the end. To achieve this, the aircraft pitches up and then down, resulting in a decrease and increase in velocity, respectively,



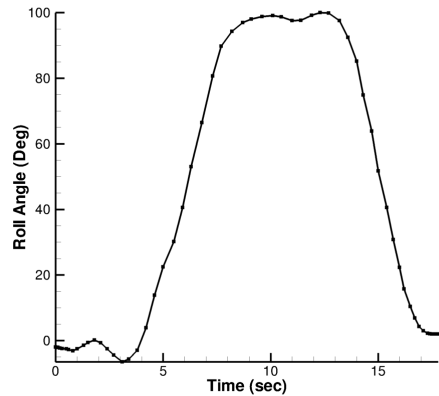
(a) Change in altitude with time.



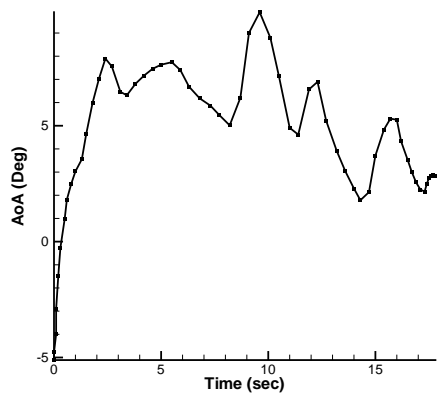
(b) Change in pitch angle with time.



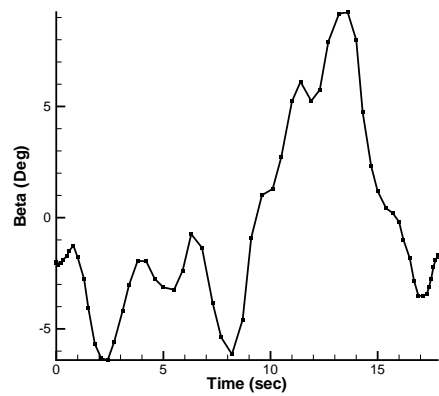
(c) Change in velocity with time.



(d) Change in bank angle with time.



(e) Change in angle of attack with time.



(f) Change in sideslip angle with time.

Figure 5. Time histories of lazy eight manoeuvre.

reaching a minimum at the top of the manoeuvre, Fig. 5(c). While the aircraft is reaching its highest altitude, it starts to roll in order to turn and face the opposite direction.

Figure 6 shows the crossplot between the tabular results for the lazy eight manoeuvre and the time-

accurate PMB results. The agreement is very good between the two sources. This was expected since the flow behaviour stays well within the linear region throughout the manoeuvre, as shown in Fig. 5(e). The smoother trend from the replay is caused by the curve fitting function introduced to increase the number of timesteps to 500, as opposed to the 40 points in the manoeuvre obtained from DIDO.

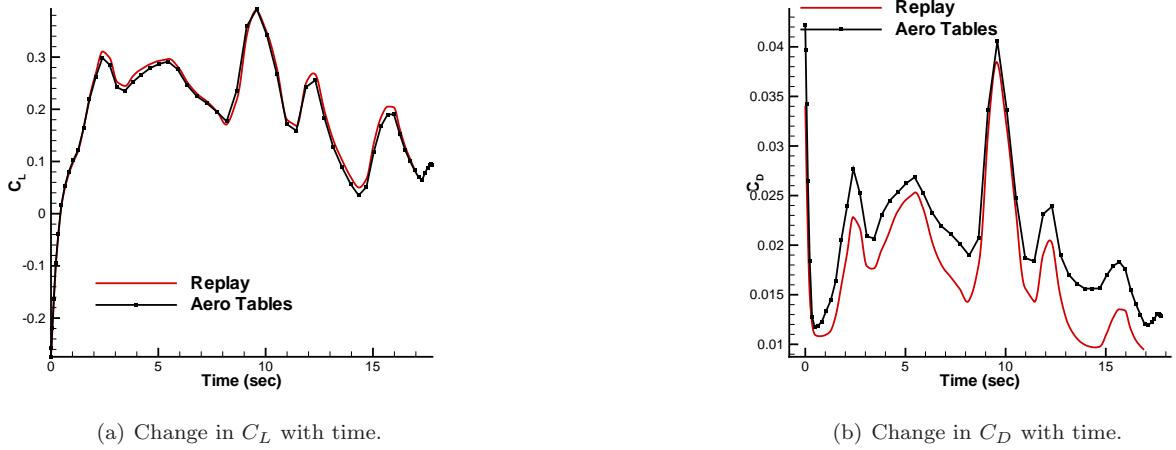


Figure 6. Comparison of tabular and time-accurate PMB calculations for the lazy eight manoeuvre.

B. Pull-up

The pull-up manoeuvre consists of an increase in altitude of around $6m$ over a period of 1 second. A schematic representation is shown in Fig. 7. The purpose of this manoeuvre is to take the aircraft through the nonlinear part of the angle of attack in a short period of time. This way, transient flow regions are expected to occur.

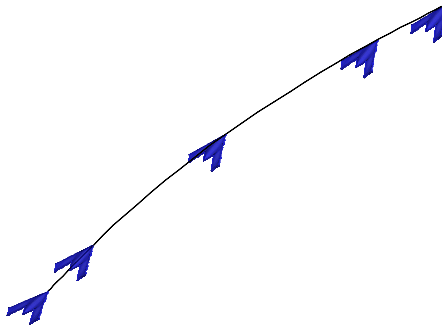
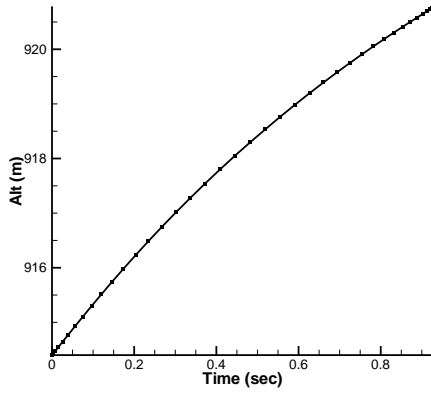


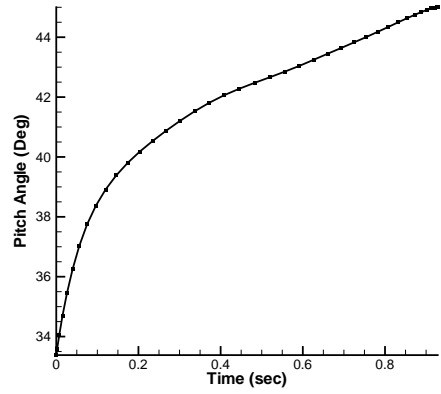
Figure 7. Lazy eight flight path.

An initial steep increase in pitch angle is seen, accomplished by thrust vectoring control, before settling at an angle of 45° . The aircraft increases in height as a consequence, shown in Fig. 8(a). Note that the angle of attack of the aircraft changes from -5° to 25° in a short period of time, going through the region of vortical flow structures and nonlinear aerodynamic behaviour. The forward velocity was set constant throughout the manoeuvre. This is a relatively simple manoeuvre with most changes occurring in the longitudinal axes.

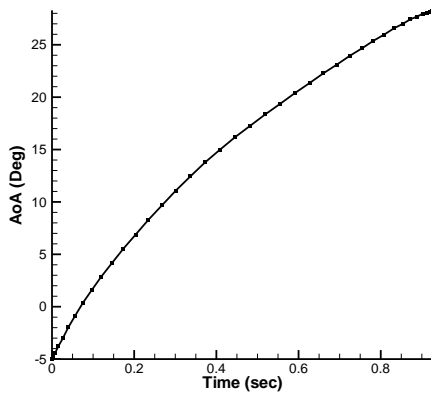
The results from the forces obtained from the tables and the manoeuvres agree during the first 0.3



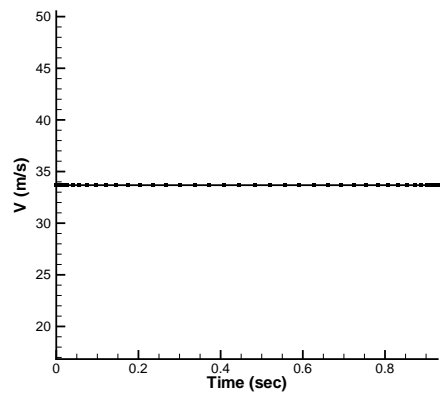
(a) Change in altitude with time.



(b) Change in pitch angle with time.



(c) Change in angle of attack with time.



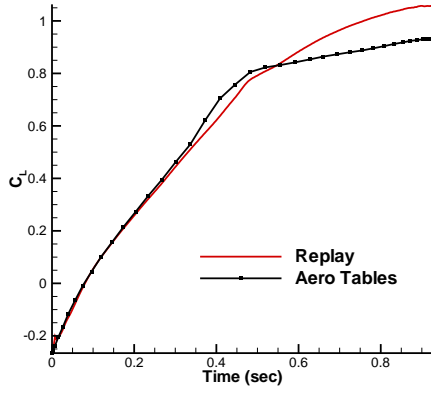
(d) Change in velocity with time.

Figure 8. Time histories of pullup manoeuvre.

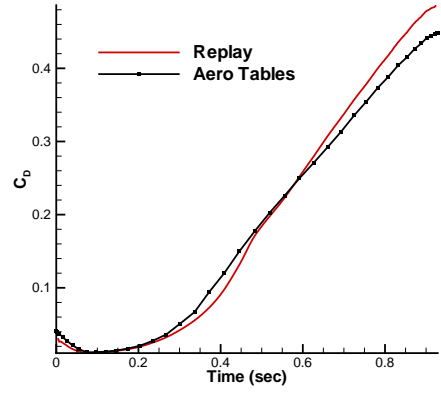
seconds, shown in Fig. 9. By inspecting Fig. 8(c), it can be seen that the incidence increases above 10° at this instance. It was described in section IV how the first vortices start to form at the tip above this incidence. As the angle of attack increases further, the apex vortex forms and could be the cause for the further disagreement beyond 0.55 seconds. Another cause for disagreement could be the lack of dynamic terms in the tables. The inclusion of such will be the focus of further study.

The conditions at 0.88 seconds were used to calculate the steady state solution at that instance. These were $\alpha = 26.3^\circ$, $M = 0.1026$ and $\beta = 0$. The flow topology predicted from this was compared to that obtained at the same instance during the replay. The surface pressure coefficient distribution is shown in Fig. 10 where differences can be seen. Overall the flow topology is very similar although the vortex breakdown position seems to be at a further upstream location in the replay solution.

In order to look at the flow solutions in more detail, slices of C_P along the chord and span were extracted and compared. The crossplots can be seen in Fig. 11. The differences in the prediction methods become more evident from this. Overall the vortices predicted by the tables are stronger. This can be expected since the aircraft is experiencing an increase in angle of attack at this instance, therefore there will be a downward component of flow in the replay. This component reduces the effective angle of attack, yielding vortices that resemble those at a lower incidence. Hence the vortex is slightly weaker throughout the flowfield.

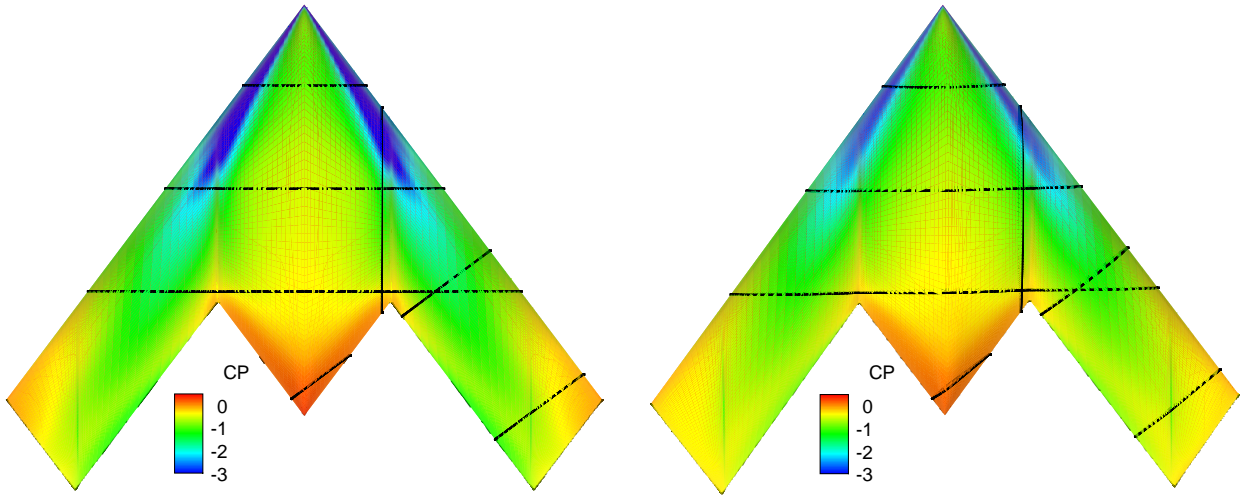


(a) Change in C_L with time.



(b) Change in C_D with time.

Figure 9. Comparison of tabular and time-accurate PMB calculations for the pullup manoeuvre.



(a) Steady state solution.

(b) Time-accurate solution.

Figure 10. Comparison of tabular and time-accurate predicted flow topologies at $\alpha = 26.3^\circ$, $M = 0.1026$ and $\beta = 0$.

VII. Conclusion

The results obtained from the manoeuvres described in this paper show the strengths of the two methods employed, tabular and time-accurate replay. The tabular method proved a cost-effective tool for manoeuvres within the linear aerodynamic regime. When the manoeuvres went into the high angle of attack regime with rapid changes in attitude, the tables showed discrepancies with the tables time accurate method. The reason for this is the capacity for the replay method to predict the flow transients that occur while large, rapid changes take place. This flow hysteresis can have a great effect on the overall forces and moments on the aircraft as was seen from the discrepancies in the pullup manoeuvre.

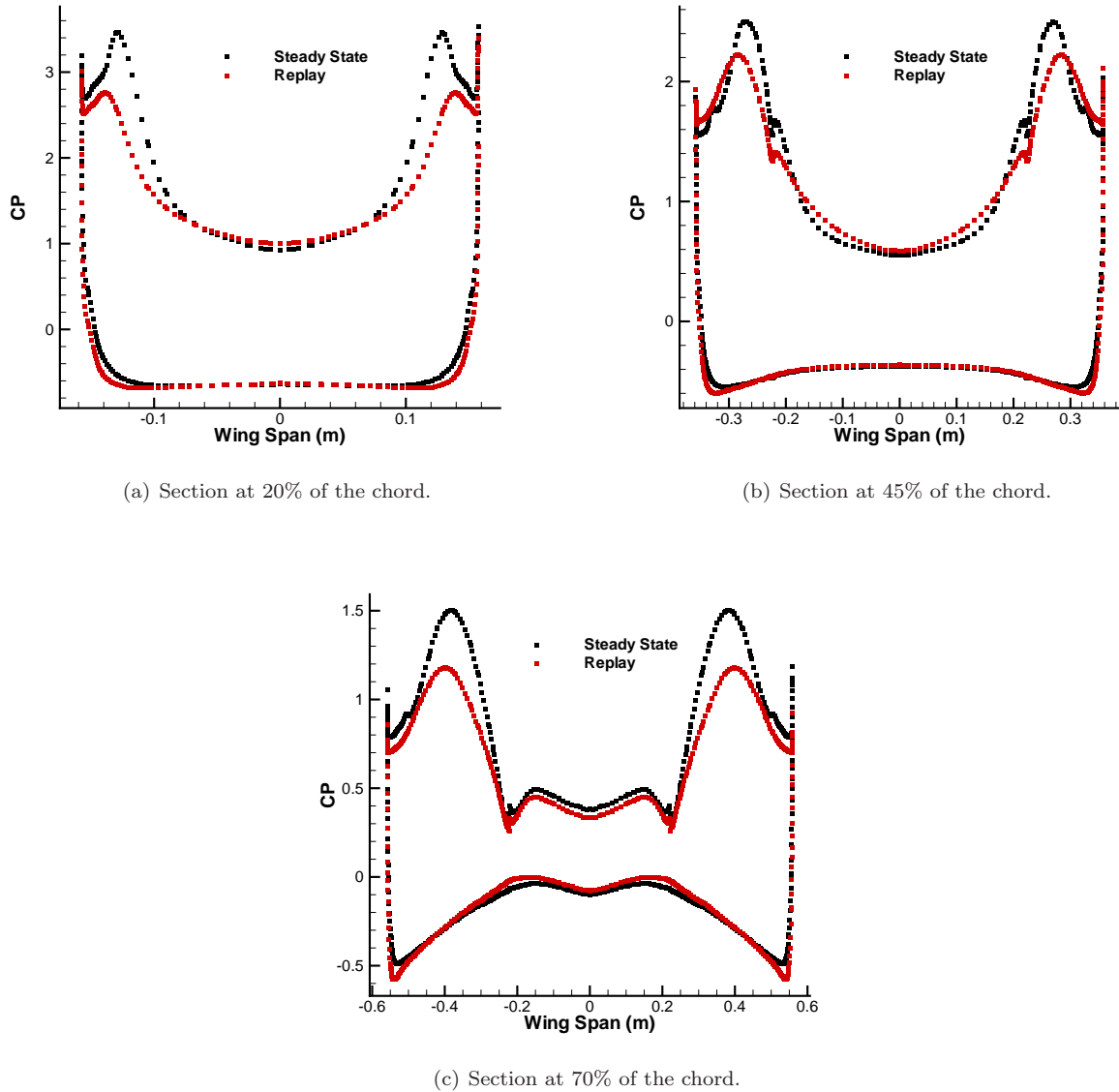


Figure 11. Comparison of tabular and time-accurate C_P predictions at $\alpha = 26.3^\circ$, $M = 0.1026$ and $= 0$.

Acknowledgments

This study is supported by an EPSRC and QinetiQ studentship. Computer time was provided though the UK Applied Aerodynamics Consortium (UKAAC) under EPSRC grant EP/F005954/1. The contribution of the Garteur AG47 group is also greatly appreciated.

References

- ¹I. Gursul, R. Gordnier, and M. Visbal. Unsteady Aerodynamics of Non slender Delta Wings. *Progress in Aerospace Sciences*, Vol. 41, 2005, pp. 515-557, doi:10.1016.
- ²M. Ghoreyshi, K. J. Badcock, A. Da Ronch, S. Marques, A. Swift, and N. Ames. Framework for Establishing the Limits of Tabular Aerodynamic Models for Flight Dynamics Analysis. *AIAA Guidance, Navigation and Control Conference*, 10-13 August 2009, Chicago, Illinois.
- ³T. Loeser, D. Vicroy, and A. Schuette. SACCON Static Wind Tunnel Tests at DNW-NWB and 14x22 NASA LaRC. *28th AIAA Applied Aerodynamics Conference*, AIAA-2010-4393, June 2010.

- ⁴ANSYS ICEM CFD. Software Package, Ver. 11.0, Ansys Inc., Southpointe, 275 Technology Drive, Canonsburg, PA 15317, U.S.A.
- ⁵K. J. Badcock, B. E. Richards, and M. A. Woodgate. Elements of Computational Fluid Dynamics on Block Structured Grids Using Implicit Solvers. *Progress in Aerospace Sciences*, Vol. 36, 2000, pp. 351-92.
- ⁶F. R. Menter. Zonal Two Equation $k-\omega$ Turbulence Models for Aerodynamic Flows. *24th AIAA Fluid Dynamics Conference*, AIAA-93-2906, July 1993.
- ⁷D. C. Wilcox. Turbulence Modelling for CFD. DCW Industries Inc., 3rd Edition, La Cañada, CA, 2006.
- ⁸D. Vallespin, A. Da Ronch, O. Boelens, and Badcock K. J. Assessment of the Limits of Tabular Aerodynamic Models for Flight Dynamics Analysis using the SACCON UCAV Configuration. *28th AIAA Applied Aerodynamics Conference*, AIAA-2010-4560, June 2010.
- ⁹A. Schuette. Numerical and Experimental Analyses of the Vortical Flow Around the SACCON Configuration. *28th AIAA Applied Aerodynamics Conference*, AIAA-2010-4690, June 2010.
- ¹⁰M. Ghoreyshy, K. J. Badcock, and M. A. Woodgate. Accelerating the Numerical Generation of Aerodynamic Models for Flight Simulation. *Journal of Aircraft*, 2009.
- ¹¹J. T. Betts. Survey of numerical methods for trajectory optimization. *Journal of Guidance, Control, and Dynamics*, Vol. 21, No. 2, pp. 193-207., 1998.
- ¹²D. G. Hull. Conversion of optimal control problems into parameter optimization problems. *Journal of Guidance, Control, and Dynamics*, Vol. 20, No. 1, pp. 57-60, 1997.
- ¹³K. Brinkman and H. G. Visser. Optimal turn-back manoeuvre after engine failure in a single-engine aircraft during climb-out. *Journal of Aerospace Engineering*, Vol. 22, Part G., 2006, pp. 17-27.
- ¹⁴F. Fahroo and I. M. Ross. Costate estimation by a legendre pseudospectral method. *Journal of guidance, control and dynamics*, Vol. 24, No.2, 2001, pp. 270- 277.
- ¹⁵I. M. Ross and F. Fahroo. User's manual for dido 2002: A matlab application package for dynamic optimization. NPS Technical Rept, Dept. of Aeronautics and Astronautics, Naval Postgraduate School, Monterey, CA, AA-02-002, 2002.
- ¹⁶Matlab version 2008a. The Mathworks, Inc., <http://www.mathworks.com>, 2008.
- ¹⁷Hussaini M. Y. Gottlieb, D. and S. A. Orszag. Theory and applications of spectral methods. 1984.
- ¹⁸Hussaini M. Y. Quarteroni A. Canuto, C. and T. A. Zang. *Spectral Methods in Fluid Dynamics*. Springer-Verlag, New York, 1988.
- ¹⁹Kazemi M. A. Elnagar, J. and M. Razzaghi. The pseudospectral legendre method for discretizing optimal control problems. *IEEE Transactions on Automatic Control*, Vol. 40, No. 10, 1995, pp. 1793-1796.
- ²⁰B. Etkin. *Dynamics of Flight, Stability and Control*. 2nd Edition. Wiley, 1982.
- ²¹B.L. Steven and F. L. Lewis. *Aircraft Control and Simulatoon*. Wiley, 1992.